Macromolecules

pubs.acs.org/Macromolecules Article

Thiazolyl-Substituted Isomeric Benzodithiophenes Boost the Photovoltaic Performance of Polymer Donors

Kangqiao Ma,† Huazhe Liang,† Yuxin Wang, Xinyuan Jia, Wendi Shi, Zhaoyang Yao,* Xiangjian Wan, Chenxi Li, and Yongsheng Chen*

Cite This: *Macromolecules* 2024, 57, 8392−8400 Read Online

ACCESS | Metrics & More | Article Recommendations | Supporting Information

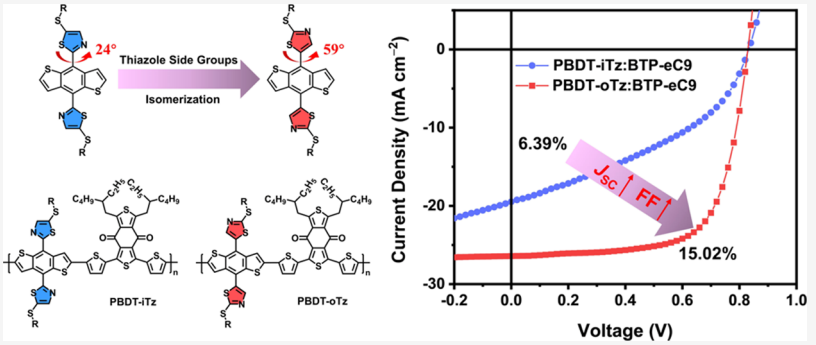

ABSTRACT: The two-dimensional side groups on benzodithiophene, especially thiophene derivatives, play a critical role in tailoring the bandgap, interchain packing, and photovoltaic outcomes of the most successful polymer donors. In light of the highly similar five-membered ring but vastly different electron-deficient properties, thiazole is expected to not only inherit the ability of the thiophene side group in conformation control but also be beneficial for constructing wide-bandgap polymer donors with deeper highest occupied molecular orbitals (HOMOs). Herein, two isomeric polymers (PBDT-oTz and PBDT-iTz) with different thiazolyl orientations on benzodithiophene are explored. A systematic investigation reveals that PBDT-oTz, featuring thiazolyl nitrogen far from benzodithiophene, achieves a deeper HOMO and appropriate molecular aggregation compared with its PBDT-iTz counterpart. Consequently, the PBDT-oTz-based device affords an excellent power conversion efficiency of 15.02%, much better than the 6.39% for PBDT-iTz. These results manifest the great effectiveness of thiazole in constructing high-performance wide-bandgap polymer donors.

Downloaded via NANKAI UNIV on September 19, 2024 at 02:29:31 (UTC).
See https://pubs.acs.org/sharingguidelines for options on how to legitimately share published articles.

INTRODUCTION

As an emerging photovoltaic technology, polymer solar cells (PSCs) have unique advantages, such as being lightweight, flexible, bendable, and easy to fabricate by low-cost solution processing.[1−5] Therefore, PSCs have aroused extensive attention from both academia and industry. Recently, profiting from the rapid development of fused-ring nonfullerene acceptors (Y series),[3,5] PSCs have significantly improved power conversion efficiencies (PCEs) by over 20%.[6] However, in sharp contrast to the plenty of high-performance nonfullerene acceptor (NFA) materials, the development of donor materials is relatively lagging behind.[7,8] The main reason is that the structure−property relationship between the polymer structure and optoelectronic properties is a challenging topic; in addition, the batch problem of polymer materials is difficult to control.[9] Currently, the most widely used polymer donor materials are PBDB-T and its derivatives. PBDB-T-type polymers include two parts: the electron-donating (D) moiety based on benzodithiophene (BDT) and the electron-accepting (A) moiety based on benzodithiophenedione (BDD).[10] In the era of fullerene acceptor, Hou and co-workers introduced the concept of two-dimensional (2D) conjugated side group on BDT units.[11,12] The study found that introducing the conjugated side groups could make polymers exhibit red-shifted absorption spectra, lower highest occupied molecular orbital (HOMO) and lowest unoccupied molecular orbital (LUMO) energy levels, better thermal stabilities, and significantly higher hole mobility, further realizing high PCE values. At present, researchers generally use thiophene and their derivatives, such as fluorinated thiophene, as the conjugated side chains of BDT. Although fluorinated thiophene is very efficient, obtaining the target monomers usually causes a tedious and costly procedure.[10] Therefore, the

Received: June 25, 2024
Revised: August 6, 2024
Accepted: August 13, 2024
Published: August 20, 2024

ACS Publications © 2024 American Chemical Society

https://doi.org/10.1021/acs.macromol.4c01474
Macromolecules 2024, 57, 8392−8400

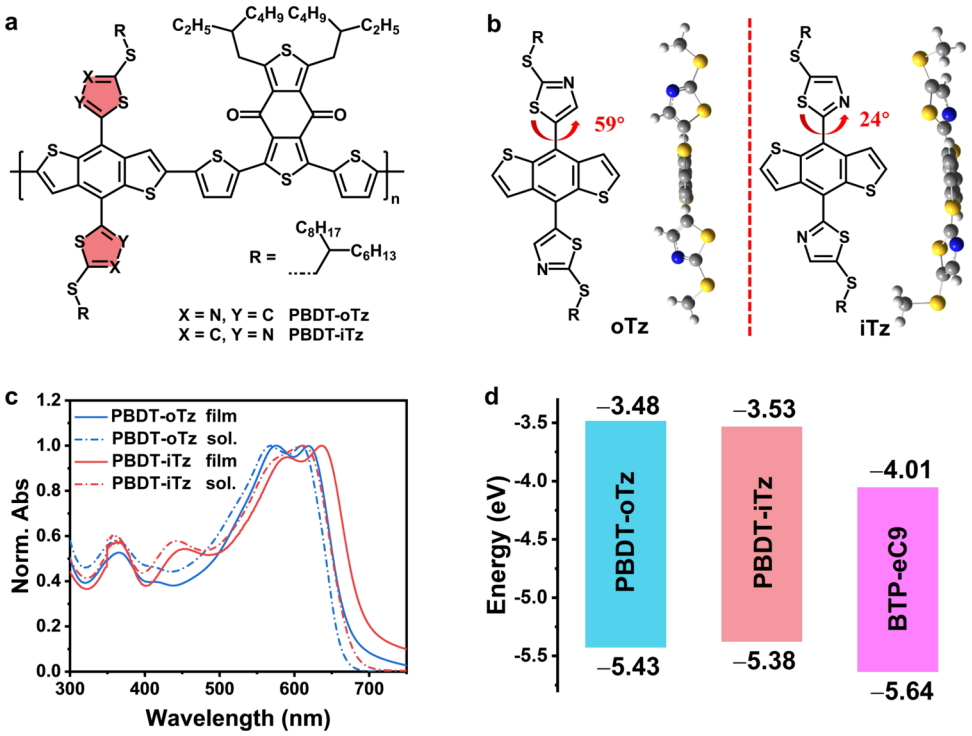

Figure 1. (a) Molecular structure of two polymer donors. (b) Optimized molecular geometries of oTz and iTz. (c) Absorption spectra of PBDT-oTz and PBDT-iTz in chloroform solutions and solid films. (d) Energy alignments of PBDT-oTz, PBDT-iTz, and BTP-eC9.

Scheme 1. Synthetic Route of Two Polymer Donors

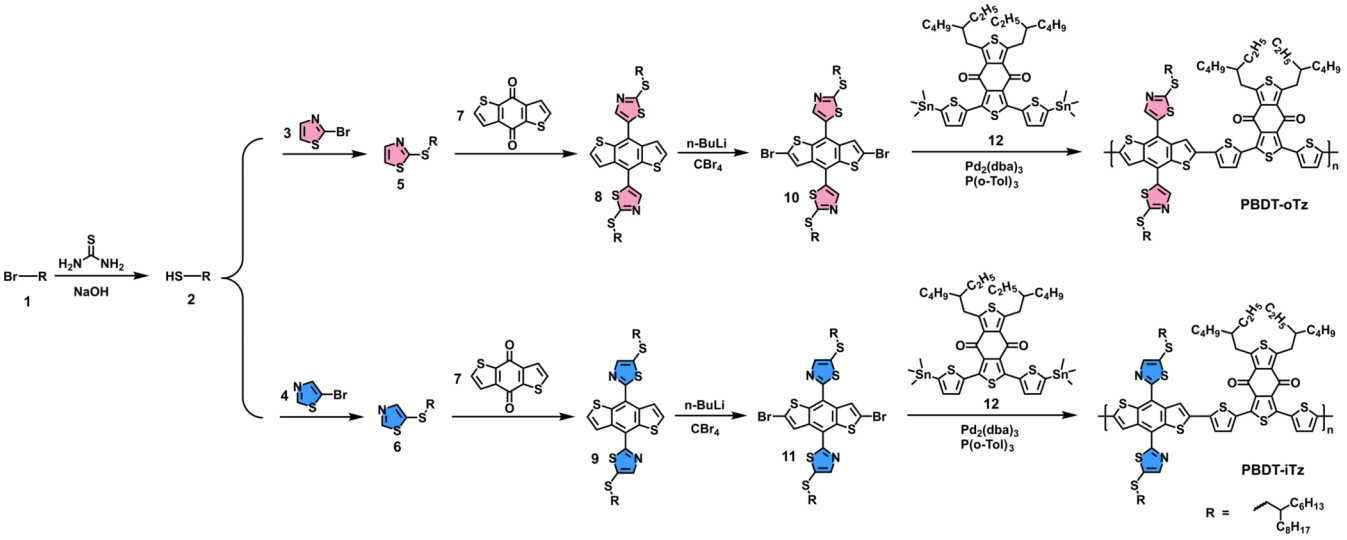

development of easier and cheaper chemical building blocks is also of great importance.

In light of the much-enhanced light absorption of NFAs compared to fullerenes, at present, it will be better if polymer donors could possess a broad absorption spectrum at short wavelengths and deep HOMO.[2,13,14] In this way, the resulting polymer donors will better match the current high-performance NFAs at the aspect of both absorption and energy levels.[5] Compared with thiophene, the thiazolyl unit has a highly similar five-membered ring but vastly different electron-deficient properties. Therefore, thiazole is expected to not only inherit the ability of the thiophene side group in conformation control but also be beneficial for constructing wide-bandgap polymer donors with deeper HOMOs, which is beneficial for obtaining larger open-circuit voltages in the resulting PSCs. However, only a few studies have reported using thiazolyl as the conjugated side group of BDTs thus far.[15] In our group's previous work, the thiazolyl-substituted BDT units were applied to construct A−D−A-type small-molecule donor materials and achieved an excellent photoelectric conversion performance.[16,17] In fact, the design principles of small molecules and polymer optoelectronic materials are interconnected. Therefore, it is also quite promising to develop highly efficient polymer donor materials based on thiazolyl side groups.

https://doi.org/10.1021/acs.macromol.4c01474
Macromolecules 2024, 57, 8392−8400

In this study, the alkylthio-substituted thiazoles were first introduced into the BDT units. As a result, two isomeric polymer donors PBDT-oTz and PBDT-iTz were afforded by adjusting the orientation of the N atom in thiazolyl rings (Figure 1a). Interestingly, despite their similar conjugated skeletons, the inherent properties of PBDT-oTz and PBDT-iTz, such as optical and aggregation properties, are markedly different. In particular, PBDT-oTz shows more blue-shifted absorptions, lower HOMO levels, and appropriate preaggregation behavior in solutions. When blended with a BTP-eC9 acceptor, the PBDT-oTz-based PSCs yield a superior PCE of 15.02%. On the contrary, the PCE of PSCs based on PBDT-iTz is quite low (only 6.39%). The success of PBDT-oTz preliminarily suggests that thiazolyl is another highly efficient conjugated side group of BDT after the thiophene and benzene rings. Furthermore, two structurally similar thiazole isomers exhibit great differences in performance, demonstrating that polymer properties can be effectively improved by adjusting the orientation of the nitrogen atom.

RESULTS AND DISCUSSION

Synthesis and Characterizations. The synthetic routes to the two polymer donors are presented in Scheme 1. Compounds 1, 3, 4, 7, and 12 were purchased and used without any additional purifications. Compound 2 was synthesized according to the literature with excellent yield.[18] Compounds 5 and 6 were synthesized through a nucleophilic substitution reaction between compound 2 and compounds 3/4. Then, compounds 5/6 and 7 underwent a Michael addition reaction to yield compounds 8 and 9. Afterward, compounds 8 and 9 were treated with trimethyltin chloride and *n*-butyllithium to obtain the corresponding stannide. Unfortunately, pure stannide cannot be obtained through recrystallization, which will affect the high-quality polymerization greatly. Therefore, we further synthesized bromides 10 and 11 from compounds 8 and 9, respectively. Finally, stepwise polymerization based on the Stille-coupling process reaction was carried out successfully between compounds 10/11 and compound 12 to afford polymer donors PBDB-oTz and PBDB-iTz, respectively. The polymerization progress was monitored by the molar amounts of monomers and the system viscosity. The ideal target polymer was obtained when the system color turned dark blue and was slightly soluble in dichloromethane. Both polymers have good solubility in chloroform and chlorobenzene. The detailed synthetic procedures are described in the Supporting Information. As shown in Figure S1, the molecular weight (M_n) and polydispersity index (PDI) of PBDT-oTz and PBDT-iTz were determined to be 43.7/3.45 and 49.4/2.59 kDa, respectively, by a high-temperature gel permeation chromatography (GPC). Thermogravimetric analysis (TGA) measurements demonstrate that the two polymers exhibit outstanding thermal stability with 5% weight loss at 350 and 354 °C for PBDT-iTz and PBDT-oTz, respectively (Figure S2).

Optical and Electrochemical Properties. To reveal the influence of the isomer-thiazolyl on the torsion of conjugated backbones, density functional theory (DFT) calculations were performed on D units (iTz and oTz) using the B3LYP/6-31G (d) level of theory. As shown in Figure 1b, the optimal conformation of oTz exhibits a dihedral angle of 59° between thiazolyl and BDT. However, iTz exhibits a significantly smaller dihedral angle of 24°, which should be attributed to smaller spatial hindrances caused by removed hydrogen atoms. The significant difference in the planarity of this conjugated skeleton may lead to significant variations in optoelectronic properties, which we will investigate in detail below. The ultraviolet−visible (UV−vis) absorption spectra of two polymers in solutions and film states are shown in Figure 1c, and the relevant data are summarized in Table 1. The PBDT-iTz shows an absorption peak at 612 nm and indistinct shoulder peaks at approximately 578 nm in diluted chloroform solutions. After the nitrogen atom is moved in thiazolyl, PBDT-oTz exhibits slightly blue-shifted absorption peaks at 609 nm and distinct shoulder peaks at 568 nm in diluted chloroform solutions. Compared to the PBDT-oTz, the PBDT-iTz shows a red-shift absorption spectrum in diluted chloroform solutions, which should result from the PBDT-iTz exhibiting a small dihedral angle between BDT and thiazolyl side groups, resulting in a better delocalization of electrons on the iTz unit.[19] In addition, the two polymers exhibit shoulder peaks at long wavelengths, which indicates that both polymers have appropriate preaggregation behavior in diluted chloroform solutions. Such polymer preaggregation is beneficial for forming pure domains with appropriate molecular packing structures in blend films.[20] In the solid film state, PBDT-iTz shows absorption peaks at 636 nm, and PBDT-oTz shows significant blue shift absorption peaks at 619 nm, which can better match with high-performance narrow bandgap acceptors currently. From the solution to film state, the absorption spectra of PBDT-oTz and PBDT-iTz show significant red shifts, which is the result of intermolecular stacking in the solid state. Note that the absorption properties of molecules in the solid film state depend not only on the molecular structure but also on the intermolecular interactions caused by the spatial configuration of molecules.[21] Therefore, the significant variation in the absorption spectra between PBDT-iTz and PBDT-oTz should be related to the planarity of the molecules. In particular, PBDT-iTz has stronger intermolecular interaction and aggregation ability than PBDT-oTz. This should be one of the reasons that PBDT-iTz has a significant red-shifted absorption spectrum compared to PBDT-oTz in solid films. The energy levels of PBDT-iTz and PBDT-oTz were also measured by employing cyclic voltammetry (CV) (Figure S3). Despite the quite different dihedral angles between thiazolyl and BDT, similar HOMO/LUMO energy levels for PBDT-iTz and PBDT-oTz could be observed, being −5.38/−3.53 and −5.43/−3.48 eV, respectively (Figure 1d and Table 1). The same acceptor unit and very similar donor unit comprising PBDT-iTz and PBDT-oTz polymers do not change their electron-donating and electron-deficient capacities greatly, which should account for the insignificant HOMOs and LUMOs. It was found that the LUMO level of PBDT-oTz was slightly higher than that of PBDT-iTz, resulting in sufficient driving force to enhance the exciton dissociation at the interfaces of the donors and acceptors. In addition, the upward

Table 1. Optical and Electrochemical Properties of PBDT-oTz and PBDT-iTz

materials	$\lambda_{max}^{sol.}$ (nm)	λ_{max}^{film} (nm)	λ_{onset}^{film} (nm)	$^{a}E_g^{opt}$ (eV)	$^{b}E_g^{cv}$ (eV)	HOMO (eV)	LUMO (eV)
PBDT-oTz	609	619	683	1.82	1.95	−5.43	−3.48
PBDT-iTz	612	636	701	1.77	1.85	−5.38	−3.53

$^{a}E_g$ is estimated by the equation $E_g = 1240/\lambda_{onset}$. $^{b}E_g$ is estimated by the difference between HOMO and LUMO energy levels.

https://doi.org/10.1021/acs.macromol.4c01474
Macromolecules 2024, 57, 8392−8400

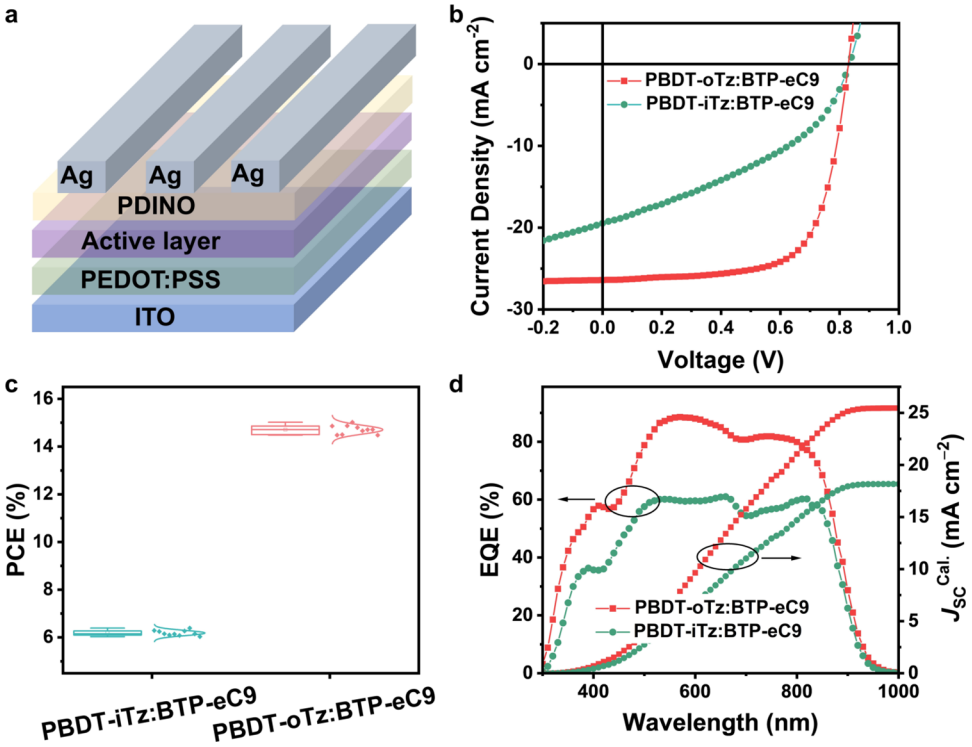

Figure 2. (a) Device structure studied here. (b) $J-V$ characteristics, (c) statistical distribution results of PCE from 10 independent devices, and (d) EQE spectra of PBDT-oTz and PBDT-iTz-based devices.

Table 2. Optimized Device Performance Data of PBDT-oTz- and PBDT-iTz-Based Devices with BTP-eC9 as Acceptor under the Illumination of 100 mW cm^{-2}[a]

active layers	V_{OC} (V)	FF (%)	J_{SC} (mA cm^{-2})	[b]$J_{SC}^{cal.}$ (mA cm^{-2})	PCE (%)
PBDT-oTz	0.830 (0.832 ± 0.006)	68.56 (68.48 ± 1.29)	26.41 (25.82 ± 0.47)	25.45	15.02 (14.81 ± 0.18)
PBDT-iTz	0.833 (0.831 ± 0.003)	39.39 (39.12 ± 0.16)	19.47 (19.03 ± 0.29)	18.17	6.39 (6.19 ± 0.11)

[a]The average photovoltaic parameters were calculated from 10 independent devices. [b]Current densities were calculated from EQE plots.

orientation of the nitrogen atoms in thiazolyl rings lowers the HOMO energy level of PBDT-oTz than PBDT-iTz. Furthermore, the PBDT-oTz exhibits a much wider electrochemistry bandgap than PBDT-iTz, which should result from the former exhibiting a more nonplanar conjugate skeleton. This is consistent with the blue-shifted absorption spectrum in the PBDT-oTz polymer.

We further tested the hole mobility of PBDT-iTz and PBDT-oTz neat films, and the results are shown in Figure S4. The hole mobility of PBDT-iTz is 1.03×10^{-3} cm^2 V^{-1} s^{-1}, while it is 7.67×10^{-4} cm^2 V^{-1} s^{-1} for PBDT-oTz. The higher hole mobility of PBDT-iTz may be due to its more planar molecular structure and enhanced intermolecular stacking.[8] Furthermore, grazing incidence wide-angle X-ray scattering (GIWAXS) experiments were implemented to reveal the stacking orientations of polymer donors. As shown in Figure S5, both polymer films exhibited observable $\pi-\pi$ stacking (010) diffraction peaks in the out-of-plane (OOP) directions, as well as lamellar stacking (100) diffraction peaks in the in-plane (IP) directions. These indicate that a face-on orientation occurred in both pristine polymer films.[22] Although the two polymers showed almost identical $\pi-\pi$ stacking distance of 3.72 Å, PBDT-iTz showed a tighter lamellar stacking distance of 25.12 Å than that of 27.30 Å for PBDT-oTz (Table S1), which may account for the higher hole mobility of PBDT-iTz.

Photovoltaic Performance. Traditional device structures (ITO/PEDOT/PSS/Polymer/BTP-eC9/PDINO/Ag) were fabricated to evaluate the photovoltaic performance of the two polymers (Figure 2a). The polymers PBDT-iTz and PBDT-oTz were used as the donor, and BTP-eC9 was selected as the acceptor.[23] We prepared the active layer of the device using both blending and layer-by-layer strategies,[24] finding that the layer-by-layer process is more suitable for our polymers (Table S2). This may be related to their strong aggregation characteristics. The optimized $J-V$ curves and device performance parameters for PBDT-iTz/BTP-eC9- and PBDT-oTz/BTP-eC9-based PSCs are exhibited in Figure 2b and Table 2. Unexpectedly, PSCs based on the more planar PBDT-iTz actually obtained an inferior PCE of 6.39% with a V_{OC} of 0.833 V, J_{SC} of 19.47 mA cm^{-2}, and FF of 39.39%. Compared with PBDT-iTz, although PBDT-oTz has suboptimal conjugate skeleton planarity, the corresponding device achieves a dramatic improvement in J_{SC} and FF after tuning the nitrogen atom position in thiazolyl, leading to a higher PCE of 15.02% (Figure 2c). These results manifested that nitrogen atom position isomerism regulation in thiazolyl is quite important to obtain more efficient polymer donors. In addition, the photoresponse spectra were evaluated by an external quantum efficiency (EQE) test. The EQE curves of PBDT-iTz/BTP-eC9 and PBDT-oTz/BTP-eC9-based devices are shown in Figure 2d. The weak photoresponse of PBDT-iTz-based

https://doi.org/10.1021/acs.macromol.4c01474
Macromolecules 2024, 57, 8392−8400

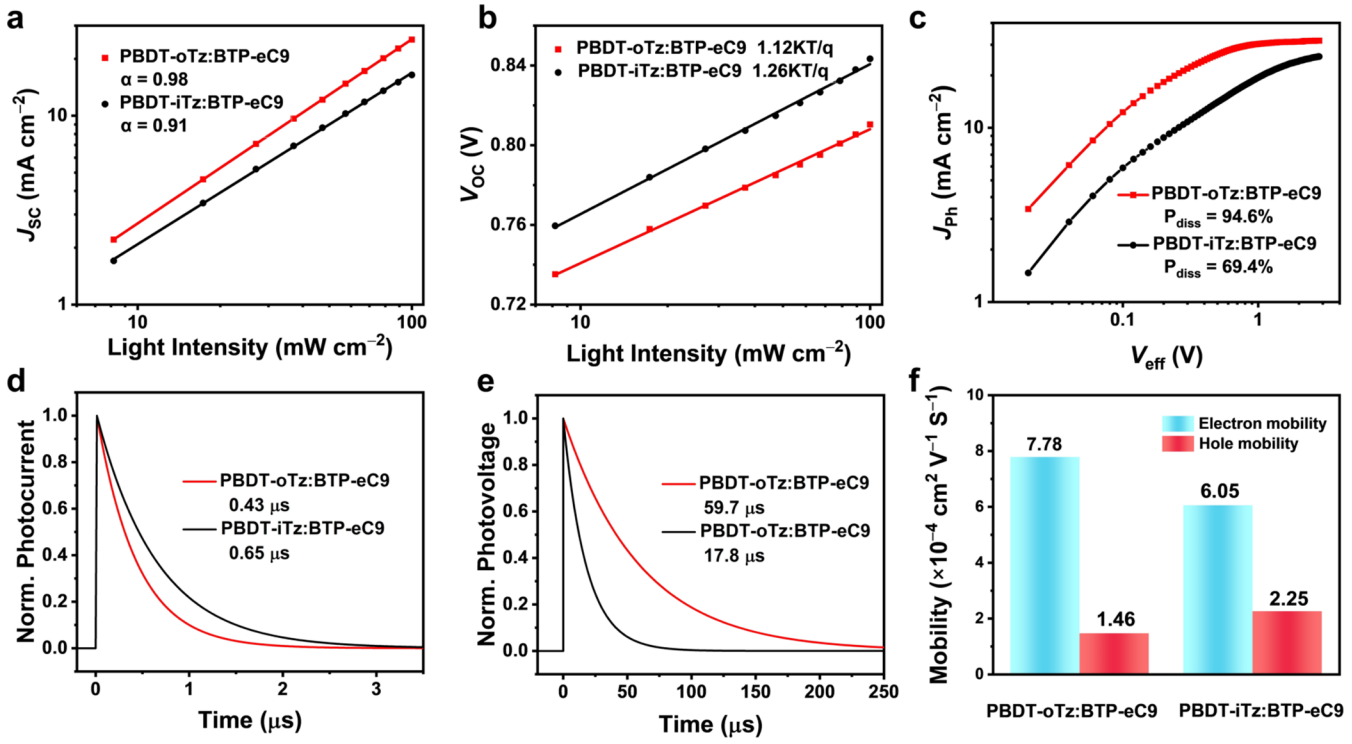

Figure 3. (a) Dependences of J_{SC} on P_{light} of optimized OSCs. (b) Dependences of V_{OC} on the P_{light} of optimized OSCs. (c) Plots of J_{ph}−V_{eff}. (d) Transient photocurrent and (d) transient photovoltage measurement for optimized OSCs. (e) Hole and electron mobilities of PBDT-oTz- and PBDT-iTz-based devices.

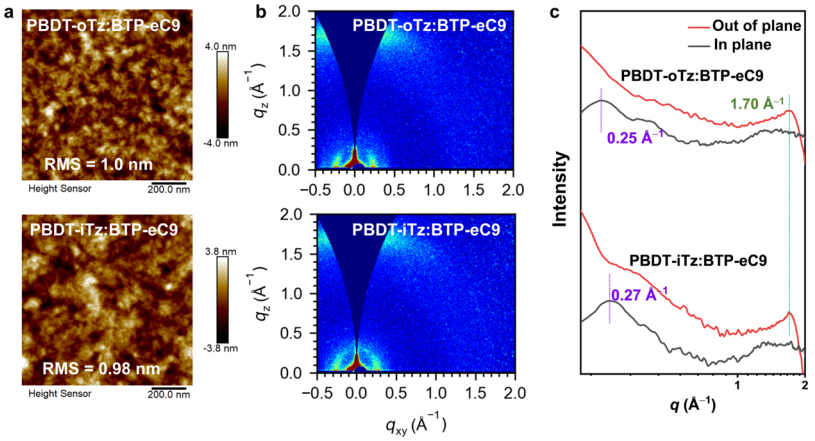

Figure 4. (a) AFM height images of PBDT-oTz and PBDT-iTz blended films. (b) 2D GIWAXS images and (c) 1D GIWAXS profiles of PBDT-oTz and PBDT-iTz blended films.

devices results in relatively low J_{SC} and performance. The better photoelectric conversion capability of PBDT-oTz-based devices should be related to the more ideal carrier dynamics transport process in the blended films.

Charge Dynamic Analysis. The charge recombination process of the two systems was investigated by measuring the J_{SC} and V_{OC} under light of different intensities (P_{light}) as shown in Figure 3a,b. The relationship between J_{SC} and P_{light} was defined as $J_{SC} \propto P_{light}^{\alpha}$, in which the value of α closing to 1 suggests lower bimolecular recombination.[25] The α values of PBDT-iTz/BTP-eC9 and PBDT-oTz/BTP-eC9 were determined to be 0.91 and 0.98, respectively. These results indicate that bimolecular recombination in the PBDT-oTz/BTP-eC9 device could be more effectively suppressed than that in PBDT-iTz-based devices. In the mensuration of the P_{light} dependence of V_{OC}, the slope value could be recognized as a reasonable estimate of the trap-state assisted charge recombination.[26] The PBDT-iTz- and PBDT-oTz-based devices showed slopes of $1.26kT/q$ and $1.12kT/q$, respectively. The smaller slope for PBDT-oTz-based devices unmasks the suppressed Shockley-Read-Hall recombination under the open-circuit condition.[27] Thus, it is reasonable that PBDT-oTz-based devices obtained higher J_{SC} and FF. Then, the photogenerated current density (J_{ph}) against effective voltage (V_{eff}) is shown in Figure 3c to reveal the behaviors of exciton dissociation. The exciton dissociation probabilities (P_{diss}) of PBDT-iTz- and PBDT-oTz-based devices can be estimated as 69.4 and 94.6%, respectively, which are consistent with the enlarged J_{SC} and FF of PBDT-oTz-based PSCs.

https://doi.org/10.1021/acs.macromol.4c01474
Macromolecules 2024, 57, 8392−8400

Transient photocurrent (TPC) and transient photovoltage (TPV) were measured to shed light on charge recombination and extraction behaviors in devices further.[28] As shown in Figure 3d, the PBDT-oTz-based device shows a slightly faster charge extraction time of 0.43 μs than the device based on PBDT-iTz (0.65 μs). The charge carrier lifetime (τ) derived from TPV measurements is 59.7 μs for PBDT-oTz/BTP-eC9, but only 17.8 μs for PBDT-oTz/BTP-eC9 (Figure 3e), suggesting greatly suppressed charge recombination in PBDT-oTz-based devices. We further resorted to SCLC to evaluate the hole (μ_h)/electron mobilities (μ_e) of PBDT-oTz- and PBDT-iTz-based blended films,[29] being 1.46×10^{-4}/7.78×10^{-4} cm^2 V^{-1} s^{-1} and 2.25×10^{-4}/6.05×10^{-4} cm^2 V^{-1} s^{-1}, respectively (Figures 3f and S6). Similar to the situation in polymer pure films, the hole mobility of PBDT-iTz blends is higher than that of PBDT-oTz blends. However, the electron mobility of PBDT-oTz blends is larger than that of PBDT-iTz blends, which may be related to the more proper phase separation in PBDT-oTz blends. In addition, the electron and hole mobilities in both devices are highly imbalanced, which may be an important reason that their efficiency is still lower than that of the current high-performance polymer donor material system.

Morphology Analysis. Atomic force microscopy (AFM) was applied to unveil the surface morphologies of the blended films. As shown in Figure 4a, both blend films exhibit similar and small root-mean-square (RMS) roughness values. Furthermore, the high image pattern of PBDT-oTz/BTP-eC9 blends exhibits more homogeneously textured aggregated clusters, suggesting better domain connectivity. However, excessive phase separation could be observed in the PBDT-iTz/BTP-eC9 blends, which may be due to the stronger aggregation property of PBDT-iTz. As illustrated in Figure S7, the phase image pattern of two blends exhibits typical fibril networks, which are beneficial for the efficient charge transfer/transport processes in theory.[7,30,31]

The 2D GIWAXS patterns of PBDT-oTz:BTP-eC9 and PBDT-iTz/BTP-eC9 blended films are shown in Figure 3b, and the corresponding one-dimensional (1D) profiles are presented in Figure 3c. Similar to the polymer donors' pristine film stacking behaviors discussed above, both system-blended films exhibit prior face-on orientation, favoring efficient charge transport in devices. Although identical $\pi-\pi$ stacking distances (3.69 Å) can be observed for PBDT-oTz and PBDT-iTz after blending with BTP-eC9, the PBDT-iTz/BTP-eC9 blends still possess a tighter lamellar stacking distance of 23.26 Å than the 25.12 Å for PBDT-oTz/BTP-eC9 blends. However, the $\pi-\pi$ stacking and lamellar stacking coherence length (CCL) for PBDT-oTz/BTP-eC9 blends is significantly larger than PBDT-iTz/BTP-eC9 blends (Table S3), suggesting more ordered molecular packings for PBDT-oTz/BTP-eC9.[32,33] These measurements could account for the more efficient charge transfer/transport dynamic processes and eventually improved photoelectric conversion performances in PBDT-oTz-based devices.[34,35]

We further performed contact angle experiments to investigate the miscibility of two polymer donors and BTP-eC9. The water and glycerol droplets on active layer pristine films are imaged in Figure S8, and the corresponding parameters, including the surface tensions (γ) and Flory–Huggins interaction parameters (χ),[36,37] are summarized in Table S4. The γ values for PBDT-oTz, PBDT-iTz, and BTP-eC9 are estimated to be 21.71, 18.43, and 28.12 mN m^{-1}, respectively. The calculated χ values for PBDT-oTz- and PBDT-iTz-based blends are 0.41, and 1.02, respectively. The smaller χ value indicates better miscibility between the donor and acceptor. Thus, the miscibility of PBDT-oTz and BTP-eC9 is better than that of PBDT-iTz and BTP-eC9, which is consistent with the increased phase separation from PBDT-oTz/BTP-eC9 to PBDT-iTz/BTP-eC9.

The energy conversion efficiency of polymer solar cells depends on V_{OC}, J_{SC}, and FF. In our study, the V_{OC} values of devices PBDT-oTz and PBDT-iTz are almost identical. However, the efficiency is significantly different due to J_{SC} and FF, which should be caused by the quite different intermolecular interactions and blended film morphology. Specifically, compared with PBDT-iTz, the conjugated skeleton of PBDT-oTz is significantly more distorted, which can prevent it from excessive aggregation. After the mixture was blended with the acceptor, appropriate phase separation was formed to obtain the more ideal carrier dynamics transport process in the blended films. However, in the PBDT-iTz-based blended films, inhibited charge generation and transport processes were obtained due to the form of excessive phase separation, ultimately leading to lower energy conversion efficiency.

Energy Losses Analysis. As we discussed above, PBDT-oTz possesses a deeper HOMO energy level compared with PBDT-iTz. However, the slightly smaller V_{OC} for PBDT-oTz:BTP-eC9-based devices can be observed. Therefore, a detailed energy loss (E_{loss}) analysis was performed and is summarized in Table S5. First, the optical bandgaps (E_g) of blended films were estimated to be 1.392 and 1.393 eV for PBDT-oTz and PBDT-iTz, respectively (Figure S9). The total E_{loss} of photovoltaic devices can be determined by the energy offset between the optical bandgap of active layer (E_g) and qV_{OC}.[38,39] Therefore, the overall E_{loss} values for PBDT-oTz- and PBDT-iTz-based devices could be calculated as 0.562 and 0.560 eV, respectively. PBDT-iTz-based devices have a slightly smaller energy loss, which should account for the corresponding device having a higher V_{OC}. Furthermore, E_{loss} can be divided into three parts ($E_{loss} = \Delta E_1 + \Delta E_2 + \Delta E_3$).[40] Resulting from very similar E_g, PBDT-oTz- and PBDT-iTz-based devices afford identical radiative recombination energy losses above the bandgap (ΔE_1) of 0.262 eV. Note that PBDT-oTz-based devices show a slightly lower radiative recombination energy loss below the bandgap (ΔE_2) of 0.050 eV compared to that of 0.067 eV for PBDT-iTz. This is generally related to the higher CT state of PBDT-oTz derived from higher LUMO levels. Lastly, the comparable nonradiative recombination energy losses (ΔE_3) for all devices based on PBDT-oTz and PBDT-iTz have been determined to be 0.250 and 0.231 eV, respectively. In addition, ΔE_3 can also be obtained from the EQE of EL (EQE_{EL}) according to the equation $\Delta E_3 = -kT\ln(EQE_{EL})$ (Figure S10).[38,41] As summarized in Table S5, the ΔE_3 values calculated from two different methods show similar variation tendencies for the two PSCs. PBDT-iTz-based devices have significantly smaller nonradiative recombination energy losses, which should derive from a closer stacking of PBDT-iTz.

CONCLUSIONS

Two isomeric polymer donors, PBDT-oTz and PBDT-iTz, were constructed by employing the thiazole unit as the conjugated side group of the BDT unit and adjusting the orientation of the N atom in the thiazolyl rings. Quite different

https://doi.org/10.1021/acs.macromol.4c01474
Macromolecules 2024, 57, 8392−8400

dihedral angles (59° for PBDT-oTz; 24° for PBDT-iTz) between thiazolyl and BDT can be afforded, which significantly affect the physicochemical properties of polymers. In particular, PBDT-oTz shows a blue-shifted absorption, down-shifted HOMO energy level, and appropriate preaggregation behavior, as well as a suitable phase separation after blending with BTP-eC9. As a result, PBDT-oTz-based devices yielded a superior PCE of 15.02%, a V_{OC} of 0.830 V, a J_{SC} of 26.41 mA cm^{-2}, and an FF of 68.56%. On the contrary, the device efficiency of PSCs based on PBDT-iTz is only 6.39%. The poor performance of PBDT-iTz-based devices is mainly due to the unsatisfactory phase separation morphology caused by excessive intermolecular interactions. Our results have manifested that thiazolyl is another highly promising conjugated side group of the BDT unit after thiophene and benzene rings. Especially, benefiting from the electron-withdrawing feature, the thiazolyl group could tune the energy levels of polymer donors effectively. Furthermore, the great importance of thiazolyl orientation relative to the BDT unit has also been revealed. Different thiazolyl orientations can significantly impact the planarity of molecules, the packing density, and the orderliness between molecules, effectively improving the photovoltaic performance of OSCs. This work could stimulate more researchers to optimize the aggregation ability of polymers by selecting appropriate thiazolyl isomers, thus providing new insights into the development of polymer donor materials.

■ ASSOCIATED CONTENT

Supporting Information

The Supporting Information is available free of charge at https://pubs.acs.org/doi/10.1021/acs.macromol.4c01474.

Brief description of detailed synthesis; material characterizations; device fabrications and measurements; calculation method; and results (PDF)

■ AUTHOR INFORMATION

Corresponding Authors

Zhaoyang Yao − *State Key Laboratory and Institute of Elemento-Organic Chemistry, The Centre of Nanoscale Science and Technology and Key Laboratory of Functional Polymer Materials, Renewable Energy Conversion and Storage Center (RECAST), College of Chemistry, Nankai University, Tianjin 300071, China;* orcid.org/0000-0003-1384-183X; Email: zyao@nankai.edu.cn

Yongsheng Chen − *State Key Laboratory and Institute of Elemento-Organic Chemistry, The Centre of Nanoscale Science and Technology and Key Laboratory of Functional Polymer Materials, Renewable Energy Conversion and Storage Center (RECAST), College of Chemistry, Nankai University, Tianjin 300071, China;* orcid.org/0000-0003-1448-8177; Email: yschen99@nankai.edu.cn

Authors

Kangqiao Ma − *State Key Laboratory and Institute of Elemento-Organic Chemistry, The Centre of Nanoscale Science and Technology and Key Laboratory of Functional Polymer Materials, Renewable Energy Conversion and Storage Center (RECAST), College of Chemistry, Nankai University, Tianjin 300071, China*

Huazhe Liang − *State Key Laboratory and Institute of Elemento-Organic Chemistry, The Centre of Nanoscale Science and Technology and Key Laboratory of Functional Polymer Materials, Renewable Energy Conversion and Storage Center (RECAST), College of Chemistry, Nankai University, Tianjin 300071, China*

Yuxin Wang − *State Key Laboratory and Institute of Elemento-Organic Chemistry, The Centre of Nanoscale Science and Technology and Key Laboratory of Functional Polymer Materials, Renewable Energy Conversion and Storage Center (RECAST), College of Chemistry, Nankai University, Tianjin 300071, China*

Xinyuan Jia − *State Key Laboratory and Institute of Elemento-Organic Chemistry, The Centre of Nanoscale Science and Technology and Key Laboratory of Functional Polymer Materials, Renewable Energy Conversion and Storage Center (RECAST), College of Chemistry, Nankai University, Tianjin 300071, China*

Wendi Shi − *State Key Laboratory and Institute of Elemento-Organic Chemistry, The Centre of Nanoscale Science and Technology and Key Laboratory of Functional Polymer Materials, Renewable Energy Conversion and Storage Center (RECAST), College of Chemistry, Nankai University, Tianjin 300071, China*

Xiangjian Wan − *State Key Laboratory and Institute of Elemento-Organic Chemistry, The Centre of Nanoscale Science and Technology and Key Laboratory of Functional Polymer Materials, Renewable Energy Conversion and Storage Center (RECAST), College of Chemistry, Nankai University, Tianjin 300071, China;* orcid.org/0000-0001-5266-8510

Chenxi Li − *State Key Laboratory and Institute of Elemento-Organic Chemistry, The Centre of Nanoscale Science and Technology and Key Laboratory of Functional Polymer Materials, Renewable Energy Conversion and Storage Center (RECAST), College of Chemistry, Nankai University, Tianjin 300071, China*

Complete contact information is available at: https://pubs.acs.org/10.1021/acs.macromol.4c01474

Author Contributions

[†]K.M. and H.L. contributed equally to this work. Y.C. and Z.Y. supervised the whole project. K.M. and Y.W. performed the synthetic work. H.L. optimized the devices and conducted the characterizations. X.J. and W.S. performed the DFT calculations. K.M. prepared the original manuscript. All authors discussed the results and commented on the manuscript.

Notes

The authors declare no competing financial interest.

■ ACKNOWLEDGMENTS

The authors gratefully acknowledge the financial support from Ministry of Science and Technology of the People's Republic of China (National Key R&D Program of China, 2022YFB4200400, 2019YFA0705900) National Natural Science Foundation of China (21935007, 52025033, 51873089), Tianjin city (22JCQNJC00530), and Haihe Laboratory of Sustainable Chemical Transformations. The authors gratefully acknowledge the cooperation of the beamline scientists at BSRF-1W1A beamline.

REFERENCES

(1) Cui, C.; Li, Y. High-Performance Conjugated Polymer Donor Materials for Polymer Solar Cells with Narrow-Bandgap Nonfullerene Acceptors. *Energy Environ. Sci.* **2019**, *12*, 3225−3246.

(2) Fu, H.; Wang, Z.; Sun, Y. Polymer Donors for High-Performance Non-Fullerene Organic Solar Cells. *Angew. Chem., Int. Ed.* **2019**, *58*, 4442−4453.

(3) Yuan, J.; Zhang, Y.; Zhou, L.; Zhang, G.; Yip, H.-L.; Lau, T.-K.; Lu, X.; Zhu, C.; Peng, H.; Johnson, P. A.; Leclerc, M.; Cao, Y.; Ulanski, J.; Li, Y.; Zou, Y. Single-Junction Organic Solar Cell with over 15% Efficiency Using Fused-Ring Acceptor with Electron-Deficient Core. *Joule* **2019**, *3*, 1140−1151.

(4) Cong, P.; Wang, Z.; Geng, Y.; Meng, Y.; Meng, C.; Chen, L.; Tang, A.; Zhou, E. Benzothiadiazole-Based Polymer Donors. *Nano Energy* **2023**, *105*, No. 108017.

(5) Wei, Q.; Yuan, J.; Yi, Y.; Zhang, C.; Zou, Y. Y6 and Its Derivatives: Molecular Design and Physical Mechanism. *Natl. Sci. Rev.* **2021**, *8*, No. nwab121.

(6) Jiang, Y.; Sun, S.; Xu, R.; Liu, F.; Miao, X.; Ran, G.; Liu, K.; Yi, Y.; Zhang, W.; Zhu, X.Non-Fullerene Acceptor with Asymmetric Structure and Phenyl-Substituted Alkyl Side Chain for 20.2% Efficiency Organic Solar Cells *Nat. Energy* 2024 DOI: 10.1038/s41560-024-01557-z.

(7) Qian, D.; Ye, L.; Zhang, M.; Liang, Y.; Li, L.; Huang, Y.; Guo, X.; Zhang, S.; Tan, Za.; Hou, J. Design, Application, and Morphology Study of a New Photovoltaic Polymer with Strong Aggregation in Solution State. *Macromolecules* **2012**, *45*, 9611−9617.

(8) Clarke, T. M.; Durrant, J. R. Charge Photogeneration in Organic Solar Cells. *Chem. Rev.* **2010**, *110*, 6736−6767.

(9) Cai, Y.; Huo, L.; Sun, Y. Recent Advances in Wide-Bandgap Photovoltaic Polymers. *Adv. Mater.* **2017**, *29*, No. 1605437, DOI: 10.1002/adma.201605437.

(10) Zheng, Z.; Yao, H.; Ye, L.; Xu, Y.; Zhang, S.; Hou, J. PBDB-T and Its Derivatives: A Family of Polymer Donors Enables over 17% Efficiency in Organic Photovoltaics. *Mater. Today* **2020**, *35*, 115−130.

(11) Ye, L.; Jiao, X.; Zhang, H.; Li, S.; Yao, H.; Ade, H.; Hou, J. 2D-Conjugated Benzodithiophene-Based Polymer Acceptor: Design, Synthesis, Nanomorphology, and Photovoltaic Performance. *Macromolecules* **2015**, *48*, 7156−7163.

(12) Huo, L.; Zhang, S.; Guo, X.; Xu, F.; Li, Y.; Hou, J. Replacing Alkoxy Groups with Alkylthienyl Groups: A Feasible Approach to Improve the Properties of Photovoltaic Polymers. *Angew. Chem., Int. Ed.* **2011**, *50*, 9697−9702.

(13) Hou, J.; Inganäs, O.; Friend, R. H.; Gao, F. Organic Solar Cells Based on Non-Fullerene Acceptors. *Nat. Mater.* **2018**, *17*, 119−128.

(14) Inganäs, O. Organic Photovoltaics over Three Decades. *Adv. Mater.* **2018**, *30*, No. 1800388.

(15) Xiao, Z.; Subbiah, J.; Sun, K.; Ji, S.; Jones, D. J.; Holmes, A. B.; Wong, W. W. H. Thiazolyl Substituted Benzodithiophene Copolymers: Synthesis, Properties and Photovoltaic Applications. *J. Mater. Chem. C* **2014**, *2*, 1306−1313.

(16) Ma, K.; Feng, W.; Liang, H.; Chen, H.; Wang, Y.; Wan, X.; Yao, Z.; Li, C.; Kan, B.; Chen, Y. Modulation of Alkyl Chain Length on the Thiazole Side Group Enables over 17% Efficiency in All-Small-Molecule Organic Solar Cells. *Adv. Funct. Mater.* **2023**, *33*, No. 2214926.

(17) Wu, S.; Feng, W.; Meng, L.; Zhang, Z.; Si, X.; Chen, Y.; Wan, X.; Li, C.; Yao, Z.; Chen, Y. 15.51% Efficiency All-Small-Molecule Organic Solar Cells Achieved by Symmetric Thiazolyl Substitution. *Nano Energy* **2022**, *103*, No. 107801.

(18) Tylleman, B.; Gbabode, G.; Amato, C.; Buess-Herman, C.; Lemaur, V.; Cornil, J.; Aspe, R. G.; Geerts, Y. H.; Sergeyev, S. Metal-Free Phthalocyanines Bearing Eight Alkylsulfonyl Substituents: Design, Synthesis, Electronic Structure, and Mesomorphism of New Electron-Deficient Mesogens. *Chem. Mater.* **2009**, *21*, 2789−2797.

(19) An, C.; Hou, J. Benzo[1,2-B:4,5-B′]Dithiophene-Based Conjugated Polymers for Highly Efficient Organic Photovoltaics. *Acc. Mater. Res.* **2022**, *3*, 540−551.

(20) Xie, B.; Zhang, K.; Hu, Z.; Fang, H.; Lin, B.; Yin, Q.; He, B.; Dong, S.; Ying, L.; Ma, W.; Huang, F.; Yan, H.; Cao, Y. Polymer Pre-Aggregation Enables Optimal Morphology and High Performance in All-Polymer Solar Cells. *Sol. RRL* **2020**, *4*, No. 1900385.

(21) Zhang, S.; Ye, L.; Zhao, W.; Liu, D.; Yao, H.; Hou, J. Side Chain Selection for Designing Highly Efficient Photovoltaic Polymers with 2d-Conjugated Structure. *Macromolecules* **2014**, *47*, 4653−4659.

(22) Alexander, H.; Wim, B.; James, G.; Eric, S.; Eliot, G.; Rick, K.; Alastair, M.; Matthew, C.; Bruce, R.; Howard, P. A Saxs/Waxs/Gisaxs Beamline with Multilayer Monochromator. *J. Phys.: Conf. Ser.* **2010**, *247*, No. 012007.

(23) Cui, Y.; Yao, H.; Zhang, J.; Xian, K.; Zhang, T.; Hong, L.; Wang, Y.; Xu, Y.; Ma, K.; An, C.; He, C.; Wei, Z.; Gao, F.; Hou, J. Single-Junction Organic Photovoltaic Cells with Approaching 18% Efficiency. *Adv. Mater.* **2020**, *32*, No. 1908205.

(24) Feng, K.; Chen, L.; Cheng, J.; Wei, W.; Liu, Y.; Xie, C.; Lu, X.; Gu, H.; Xiong, S.; Zhou, Y. Understanding the Composition of Layer-by-Layer Deposited Active Layer at Buried Bottom Surface. *Adv. Funct. Mater.* **2023**, *33*, No. 2214956.

(25) Kyaw, A. K. K.; Wang, D. H.; Gupta, V.; Leong, W. L.; Ke, L.; Bazan, G. C.; Heeger, A. J. Intensity Dependence of Current−Voltage Characteristics and Recombination in High-Efficiency Solution-Processed Small-Molecule Solar Cells. *ACS Nano* **2013**, *7*, 4569−4577.

(26) Sun, Y.; Nian, L.; Kan, Y.; Ren, Y.; Chen, Z.; Zhu, L.; Zhang, M.; Yin, H.; Xu, H.; Li, J.; Hao, X.; Liu, F.; Gao, K.; Li, Y. Rational Control of Sequential Morphology Evolution and Vertical Distribution toward 17.18% Efficiency All-Small-Molecule Organic Solar Cells. *Joule* **2022**, *6*, 2835−2848.

(27) Ryu, S.; Ha, N. Y.; Ahn, Y. H.; Park, J.-Y.; Lee, S. Light Intensity Dependence of Organic Solar Cell Operation and Dominance Switching between Shockley−Read−Hall and Bimolecular Recombination Losses. *Sci. Rep.* **2021**, *11*, No. 16781.

(28) Chong, K.; Xu, X.; Meng, H.; Xue, J.; Yu, L.; Ma, W.; Peng, Q. Realizing 19.05% Efficiency Polymer Solar Cells by Progressively Improving Charge Extraction and Suppressing Charge Recombination. *Adv. Mater.* **2022**, *34*, No. 2109516.

(29) Azimi, H.; Senes, A.; Scharber, M. C.; Hingerl, K.; Brabec, C. J. Charge Transport and Recombination in Low-Bandgap Bulk Heterojunction Solar Cell Using Bis-Adduct Fullerene. *Adv. Energy Mater.* **2011**, *1*, 1162−1168.

(30) Zhang, S.; Qin, Y.; Zhu, J.; Hou, J. Over 14% Efficiency in Polymer Solar Cells Enabled by a Chlorinated Polymer Donor. *Adv. Mater.* **2018**, *30*, No. 1800868.

(31) Huang, W.; Li, M.; Zhang, L.; Yang, T.; Zhang, Z.; Zeng, H.; Zhang, X.; Dang, L.; Liang, Y. Molecular Engineering on Conjugated Side Chain for Polymer Solar Cells with Improved Efficiency and Accessibility. *Chem. Mater.* **2016**, *28*, 5887−5895.

(32) Gu, X.; Zhou, Y.; Gu, K.; Kurosawa, T.; Guo, Y.; Li, Y.; Lin, H.; Schroeder, B. C.; Yan, H.; Molina-Lopez, F.; Tassone, C. J.; Wang, C.; Mannsfeld, S. C. B.; Yan, H.; Zhao, D.; Toney, M. F.; Bao, Z. Roll-to-Roll Printed Large-Area All-Polymer Solar Cells with 5% Efficiency Based on a Low Crystallinity Conjugated Polymer Blend. *Adv. Energy Mater.* **2017**, *7*, No. 1602742.

(33) Chen, Y.; Zhu, Y.; Yang, D.; Luo, Q.; Yang, L.; Huang, Y.; Zhao, S.; Lu, Z. Asymmetrical Squaraines for High-Performance Small-Molecule Organic Solar Cells with a Short Circuit Current of over 12 mA cm^{-2}. *Chem. Commun.* **2015**, *51*, 6133−6136.

(34) Han, L.; Fan, H.; Zhu, Y.; Wang, M.; Pan, F.; Yu, D.; Zhao, Y.; He, F. Precisely Controlled Two-Dimensional Rhombic Copolymer Micelles for Sensitive Flexible Tunneling Devices. *CCS Chem.* **2021**, *3*, 1399−1409.

(35) Zhao, Q.; Lai, H.; Chen, H.; Li, H.; He, F. H- and J-Aggregation Inspiring Efficient Solar Conversion. *J. Mater. Chem. A* **2021**, *9*, 1119−1126.

(36) Wang, Q.; Li, M.; Peng, Z.; Kirby, N.; Deng, Y.; Ye, L.; Geng, Y. Calculation Aided Miscibility Manipulation Enables Highly Efficient Polythiophene:Nonfullerene Photovoltaic Cells. *Sci. China: Chem.* **2021**, *64*, 478−487.

https://doi.org/10.1021/acs.macromol.4c01474
Macromolecules 2024, 57, 8392−8400

(37) Wang, T.; Brédas, J.-L. Organic Photovoltaics: Understanding the Preaggregation of Polymer Donors in Solution and Its Morphological Impact. *J. Am. Chem. Soc.* **2021**, *143*, 1822−1835.
(38) Chen, X.-K.; Qian, D.; Wang, Y.; Kirchartz, T.; Tress, W.; Yao, H.; Yuan, J.; Hülsbeck, M.; Zhang, M.; Zou, Y.; Sun, Y.; Li, Y.; Hou, J.; Inganäs, O.; Coropceanu, V.; Bredas, J.-L.; Gao, F. A Unified Description of Non-Radiative Voltage Losses in Organic Solar Cells. *Nat. Energy* **2021**, *6*, 799−806.
(39) Qian, D.; Zheng, Z.; Yao, H.; Tress, W.; Hopper, T. R.; Chen, S.; Li, S.; Liu, J.; Chen, S.; Zhang, J.; Liu, X.-K.; Gao, B.; Ouyang, L.; Jin, Y.; Pozina, G.; Buyanova, I. A.; Chen, W. M.; Inganäs, O.; Coropceanu, V.; Bredas, J.-L.; Yan, H.; Hou, J.; Zhang, F.; Bakulin, A. A.; Gao, F. Design Rules for Minimizing Voltage Losses in High-Efficiency Organic Solar Cells. *Nat. Mater.* **2018**, *17*, 703−709.
(40) Rau, U.; Blank, B.; Müller, T. C. M.; Kirchartz, T. Efficiency Potential of Photovoltaic Materials and Devices Unveiled by Detailed-Balance Analysis. *Phys. Rev. Appl.* **2017**, *7*, No. 044016.
(41) Nikolis, V. C.; Benduhn, J.; Holzmueller, F.; Piersimoni, F.; Lau, M.; Zeika, O.; Neher, D.; Koerner, C.; Spoltore, D.; Vandewal, K. Reducing Voltage Losses in Cascade Organic Solar Cells While Maintaining High External Quantum Efficiencies. *Adv. Energy Mater.* **2017**, *7*, No. 1700855.

https://doi.org/10.1021/acs.macromol.4c01474
Macromolecules 2024, 57, 8392−8400